Correlations in Electron–Atom Collisions involving Polarised Electrons and Photons*

G. F. Hanne

Laser Atomic Physics Laboratory, School of Science,
Griffith University, Nathan, Qld 4111, Australia.
Permanent address: Physikalisches Institut, Universität Münster,
Wilhelm-Klemm-Str. 10, 48149 Münster, Germany.

Abstract

More sophisticated experimental methods to study inelastic electron–atom collisions include polarisation-correlation measurements such as electron–photon (e, eγ) and electron–electron (e, 2e) coincidence studies or stepwise electron–photon (eγ, γ) correlations. Electron correlations and spin effects can be explored on the most fundamental level in such experiments. In this paper recent (e, eγ) studies with Hg and Xe, (eγ, γ) studies with Ne and (e, 2e) studies with Xe using polarised electrons and/or polarised photons are reviewed.

1. Introduction

Excitation and ionisation of atomic and molecular targets by electron impact are important processes in gas discharges, plasmas, etc. In the past, a variety of investigations have been performed to study such processes in some detail. More sophisticated experimental methods to study inelastic electron–atom collisions include polarisation-correlation measurements such as those listed below:

- Optical Methods:
  Integrated Stokes Parameters
  Laser Excited Targets (Superelastic Scattering)
  Electron–Photon (e,2γ) Coincidences (Generalised Stokes Parameters)
  Stepwise Electron–Photon (eγ, γ) Excitation
- Triple Differential Cross Section (e, 2e) Measurements
- Generalised S T U Parameters
- Spin Asymmetries with Polarised Targets.

Whereas spin asymmetries in low energy elastic and inelastic collisions of polarised electrons with unpolarised or polarised atoms have been studied for about 35 years, only recent experimental progress has made feasible electron–photon (e, eγ) and electron–electron (e, 2e) coincidence studies involving polarised electrons. Sources of polarised electrons with a polarisation of $P \geq 0 \cdot 7$ and currents of up to several μamps have been developed with which such investigations can be performed successfully. Spin effects in elastic and inelastic collisions of electrons with atomic and molecular targets can be explored on the most fundamental level in such experiments.

10.1071/PH98087   0004-9506/99/030377$10.00

In this paper recent experimental work on spin-resolved (e, eγ) coincidences with Hg and Xe, spin-resolved triple differential (e, 2e) cross sections in Xe and (eγ, γ) correlations in Ne involving polarised photons is reviewed. The origin of the observed spin asymmetries (caused by exchange effects, spin–orbit interaction of the continuum electrons and spin–orbit coupling within the target in conjunction with orbital orientation and exchange) is explained in some detail.

2. General Background

(2a) Experimental Methods

Our goal is to disentangle the various scattering channels and interactions that govern the collisions. How can we probe collisions of electrons with atoms on the most fundamental level, i.e. as detailed as possible? The answer is illustrated in Fig. 1: We must perform a state selection before and after scattering! Thus we should not only use a polarised incident electron beam, but also state-selected targets before the collision. The system forms a collision complex, and scattered electrons with a polarisation different to that of the incident beam may be obtained. Also the target will be left in quite different states including excited or ionised states with some angular momentum orientation and alignment. Photons or electrons that are emitted from the target can be observed in coincidence with the scattered electrons which allows one to probe the final channels in great detail. However, it is not feasible to date to measure the electron polarisation after scattering in a coincidence experiment, because the efficiency of such detectors is too small to give reasonably high coincidence signals. If the excited atom is in a metastable state one may use the method of stepwise electron–photon excitation to induce fluorescence from which the population of the metastable state can be determined.
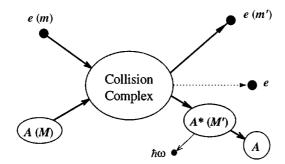

Fig. 1.   Scheme for state selected electron–atom collisions.

(2b) Scattering Amplitudes and Observables

How can we describe all this in formal terms? All observables can be expressed by complex scattering amplitudes,

$$\langle J'M'\boldsymbol{k}'m|\boldsymbol{T}|JM\boldsymbol{k}m\rangle\,, \qquad (1)$$

that are characterised by the quantum numbers of the initial and final states involved. Here J and M are the total angular momentum and magnetic quantum

number of the target before scattering, and $\boldsymbol{k}$ and m the wave vector and magnetic spin quantum number of the incident electron respectively. The primes denote the corresponding quantities after scattering. The description of a simple transition from a target state with angular momentum $J = 0$ to a final state with angular momentum $J = 1$ may require up to six different complex amplitudes, i.e. up to eleven independent parameters! It is obvious that a complete experimental determination of all required parameters is painful work, and there are only few examples (for systems requiring only two amplitudes) for which that goal has been achieved.

The observables that we deal with here are spin asymmetries and light polarisation components. We do not discuss scattering from state selected targets and generalised STU parameter measurements where the polarisation of scattered electrons is determined.

A spin asymmetry is obtained if the intensity for a process with polarisation of the incident electrons parallel to a preferential direction is different from that for polarisation antiparallel to this direction. Such preferential directions can be the polarisation vector of polarised targets or the normal to a reaction plane. Very often we can observe a spin up–down asymmetry with respect to a direction perpendicular to the scattering plane. If we denote this direction with the y axis (the incident beam direction is then the quantisation axis z), the spin up–down asymmetry is given by

$$A = \frac{I(+P_y) - I(-P_y)}{I(+P_y) + I(-P_y)} = P_y S_A\,, \qquad (2)$$

where $I(\pm P_y)$ is the intensity with polarisation $\pm P_y$ and S_A is the asymmetry function for $P_y = 1$.

A scheme of the orientation of polarisation filters for the determination of light polarisation components (Stokes parameters) is shown in Fig. 2. We can map the excited target by means of a photon detector that looks perpendicular to the incident beam direction. Light emitted along a particular direction is characterised by light polarisation components P_i (Stokes parameters):

$$P_1 = \frac{I(0°) - I(90°)}{I(0°) + I(90°)} = \eta_3,$$

$$P_2 = \frac{I(45°) - I(135°)}{I(45°) + I(135°)} = \eta_1,$$

$$P_3 = \frac{I(-) - I(+)}{I(+) + I(-)} = -\eta_2\,, \qquad (3)$$

where $I(\alpha)$ denotes the intensity transmitted by a linear polarisation filter oriented at one of the angles α shown in Fig. 2, and $I(+)$ or $I(-)$ is the intensity through filters for light with positive or negative helicity. The z axis is normally the direction of the incident electron beam. The light polarisation components (3) depend, in general, on the electron polarisation vector $\boldsymbol{P}_e$.
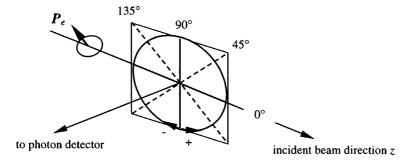
Fig. 2. Alignment and orientation of polarisation filters for Stokes parameter measurements.

(2c) Nature of Spin Effects

The spin of the colliding electrons is involved in two ways: exchange and the Pauli principle makes the cross sections dependent on the relative orientation of the spins of the colliding electrons, whereas the spin–orbit interaction is an explicit spin-dependent force that results in a fine-structure interaction within the target and Mott scattering effects for the continuum electron.

We can distinguish three different situations:

(i) The spin–orbit interaction of the entire system (continuum electrons plus target electrons) is so small that it does not influence the collision process. In that case spin effects are only caused by exchange, and LS coupling holds for the entire system. If the collisions lead to transitions between certain target states that belong to a fine-structure multiplet the (small) spin–orbit splitting is accounted for by an angular-momentum coupling procedure. In an experiment, we may resolve the fine-structure splitting and observe spin asymmetries as a result of the interplay between collisionally induced orbital orientation and exchange (the 'fine-structure effect').

(ii) We assume that the spin–orbit interaction of the continuum electron is still negligible. A weak violation of LS coupling in the target can be accounted for by a description in the intermediate-coupling scheme, where the different fine-structure states have approximately the same radial wave functions. Spin effects are still caused only by exchange, but LS coupling is violated for the entire system. An example of such a situation are the $2p^6$–$2p^5 3s$ transitions in Ne $(Z = 10)$ where an intermediate-coupling scheme applies.

In certain situations, e.g. at high energies and small scattering angles, exchange is negligible and, thus, the scattering is not spin dependent. In that case no effect from the violation of LS coupling is *observed*. But this, of course, does not mean that LS coupling holds in this case; the target states must always be described in the intermediate-coupling scheme.

(iii) The LS coupling in the target is strongly violated, so that in the description of fine-structure states not only an intermediate-coupling scheme but also different radial wave functions must be used for different fine-structure states. This will result in a deviation from statistical branching ratios and, therefore, the violation of LS coupling should be observed at all energies. For such scattering systems the spin–orbit interaction of the continuum electrons is likely to be important as well giving rise to Mott scattering effects and, consequently, even more significant

deviations from LS coupling. This could be an adequate description for the heavy targets Xe and Hg.

Case (i) results in certain relationships for spin-dependent observables that are only valid in LS coupling. Thus a violation of LS coupling results in a violation of such relationships which can be observed experimentally. However, it is, in general, difficult to distinguish case (ii) from case (iii).

There are a number of investigations in which polarised electrons and photons have been used to probe collisions in some detail. We cannot review here all these activities, but shall concentrate on only a few examples to highlight recent advances and the potential of these methods.
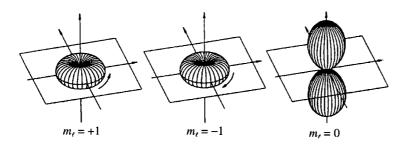

$m_\ell = +1$ $m_\ell = -1$ $m_\ell = 0$

Fig. 3. Spherical orbital sublevels of an atomic p state.

3. Optical Methods

A powerful tool to probe spin-dependent inelastic collisions are optical methods. In inelastic collisions, the magnetic sublevels of the target may show an anisotropic population. The resulting excited state is, in general, a superposition of these sublevels, where coupling to the spins is also involved (spin–orbit coupling). The orbital sublevels of an excited p state are shown in Fig. 3. The superposition of these orbitals will, in general, result in an anisotropic shape and in an orientation of the charge-cloud distribution of the excited target electrons; an example is shown in Figs 5 and 6.
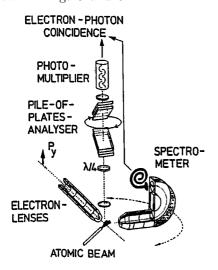

ELECTRON – PHOTON
COINCIDENCE

PHOTO-
MULTIPLIER

PILE-OF-
PLATES-
ANALYSER

P_y

$\lambda/4$

SPECTRO-
METER

ELECTRON-
LENSES

ATOMIC BEAM

Fig. 4. Scheme for an electron–photon coincidence experiment with polarised electrons. The source of polarised electrons is similar to that shown in Fig. 15.
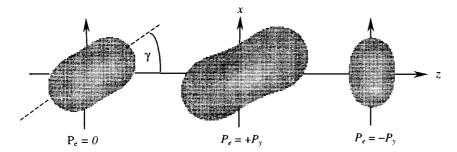
Fig. 5. Measured charge-cloud distributions for Hg*(6 ^{3}P$_1$) atoms after electron-impact excitation with polarised electrons at $E = 8$ eV and $\vartheta = 20°$ (Sohn and Hanne 1992). The z axis is the incident beam direction. The view is perpendicular to the scattering plane.

Such an ensemble of excited atoms will, in general, emit polarised light, where the linear polarisation components will give us a picture of the shape of the charge cloud, i.e. the alignment, whereas the circular polarisation components will tell us something about the target orientation after scattering. We are particularly interested in how the incident electron's spin affects the resulting charge-cloud distribution.

(3a) Electron–Photon Coincidences

If we detect scattered electrons and emitted photons in coincidence, we will select excited atoms that have scattered the electrons into a particular direction. Fig. 4 shows a scheme of our apparatus with which such experiments have been performed. We can map the excited target by means of a photon detector that looks perpendicular to the scattering plane and another detector—not shown here—that looks parallel to the scattering plane. The coincidence rates $\dot{N}(\boldsymbol{P}_e, \alpha)$ thus obtained depend on the electron polarisation $\boldsymbol{P}_e$ and the angle α of the linear polariser. A quarter wave plate in front of the linear polariser enables us to determine the coincidence rate for photons with positive and negative helicity as well. From these coincidence rates a variety of linear and circular light polarisation components (generalised Stokes parameters, see Andersen *et al.* 1997) and various spin asymmetries can be determined.

We did such experiments with Hg and Xe atoms and some examples are discussed in the following.

Electron–photon coincidences with Hg. In Fig. 5 we show some results of experimentally determined charge-cloud distributions for Hg (Sohn and Hanne 1992). We studied the excitation of the 6 ^{3}P$_1$ state of Hg at 8 eV. The excitation energy of this famous Franck–Hertz transition is about 4·9 eV, and thus the electrons are scattered with a final energy of about 3·1 eV. The scattering angle is 20°.

It is clearly seen that the shape of the resulting charge cloud of the excited target electron depends strongly on the spin orientation of the incident electron. Also the alignment angle γ through which the charge cloud is tilted from the incident electron beam direction is strongly dependent on the initial spin orientation. The size of the charge cloud distribution is a measure of the excitation cross section. So these distributions indicate also the magnitude of the cross sections

for electrons with spin up and spin down. The average of the two charge cloud distributions gives the distribution for unpolarised electrons.

The charge cloud shown in Fig. 6 is the result of the same excitation process, but now with incident electrons polarised parallel to the x direction (in the scattering plane). An explicit spin-dependent force that leads to a violation of LS coupling causes here a tilt of the charge cloud out of the scattering plane by an angle δ. However, no simple picture exists for this process, because the interplay between exchange and small spin–orbit forces (not violating LS coupling) is not sufficient for an explanation of this observation.
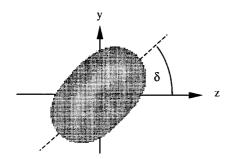

Fig. 6. Measured charge-cloud distributions for Hg*(6 $^3P_1$) atoms after electron-impact excitation at $E = 8$ eV and $\vartheta = 20°$ with electrons polarised parallel to the x direction, i.e. parallel to the scattering plane (Sohn and Hanne 1992). The view is parallel to the scattering plane.

For a comparison with theoretical data such charge-cloud plots are not well suited, but a variety of appropiate parameters can be evaluated. If the analyser is aligned such that photons that are polarised parallel or perpendicular to the incident beam direction (the quantisation axis in our description) are detected, the transitions obey the selection rule $\Delta M = 0$ or ± 1 respectively. Because we have a $J = 0 \rightarrow J = 1$ transition, the excitation of the $M = 0$ or ± 1 states is thus selected. With these polariser settings the spin up–down asymmetries $A_{||}$ and $A_\perp$ (cf. equation 2) of the coincidence rate, as well as the linear polarisation η_3 for unpolarised electrons (cf. equation 3), can be obtained. These observables can be expressed in terms of five normalised state multipoles (Goeke *et al.* 1989), so that their measurements for two different directions of the photon analyser (perpendicular and parallel to the scattering plane) yields six observables for a redundant determination of the five state multipoles. From these five state multipoles thus obtained we can evaluate other parameters, such as the scattering asymmetry $A = S_A(M)$ (cf. equation 2) for excitation of the sublevels with $M = 0$ or $M = \pm 1$, now averaged over all photon emission angles. Similarly, we can determine the spin polarisation $P = S_P(M)$ that electrons scattered from an initially unpolarised beam would acquire if the excitation of the sublevels with $M = 0$ or $M = \pm 1$ were selected. It is worth noting that $S_P(M)$ can be determined without really measuring the polarisation of the scattered electrons!

The result of such an evaluation of the measurement of Goeke *et al.* (1989) is shown in Fig. 7 for $E = 8$ eV. Quite different asymmetries are observed for the different sublevels. The theoretical curves—an R-matrix close-coupling calculation by Bartschat (1988, 1989)—show that such a detailed spin-dependent process is fairly well described by this method, whereas a distorted-wave approach (Bartschat *et al.* 1985; Bartschat 1988)—not shown here—fails completely to describe these data.
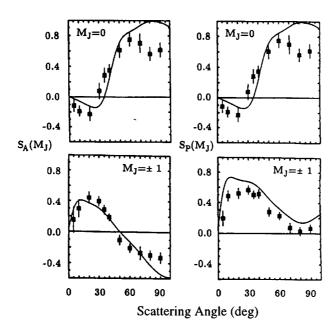
Fig. 7. Scattering asymmetry $S_A(M)$ of a totally polarised electron beam and polarisation $S_P(M)$ after scattering of initially unpolarised electrons for excitation of the sublevels $M = 0$ or ± 1 of Hg*(6 $^3P_1$) at $E = 8$ eV. Experiment: Goeke *et al.* (1989); theory: R-matrix calculation by Bartschat (1988, 1989).
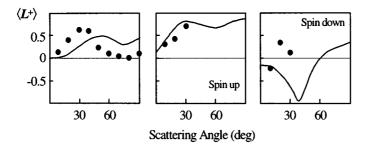

Fig. 8. Spin-resolved orientation for excitation of Hg (6 $^3P_1$ state) (Andersen *et al.* 1996).

On the other hand, from measurements of the circular polarisation, we can extract the orientation of the target electrons, and this orientation is plotted in Fig. 8 as a function of scattering angle for the two different spin orientations of the incident electrons.

For $s \to p$ transitions there exists an orientation propensity rule that states that the orientation $\langle L^+ \rangle$ of a charge cloud is positive for scattering of unpolarised electrons by small angles. This propensity rule is obviously not valid for spin-resolved collisions where the electron spin is initially down: A careful analysis of our data by Andersen *et al.* (1996) shows that in the case of the 6 $^3P_1$ excitation of Hg spin flips are very likely for spin-down electrons, but those

spin-down electrons whose spin is not flipped tend to transfer a negative angular momentum to the atom! This is indicated in Fig. 8. Unfortunately, only a few data points are available for the spin-resolved orientation parameter. Urged on by the theoretical groups, we plan to revive that investigation.

   Electron–photon coincidences with Xe.   First results for similar experiments for Xe have been obtained by Uhrig *et al.* (1994) and Berkemeier (1994). The excitation of the $5p^6 6s[\frac{3}{2}]_1 (^3P_1)$ state was investigated. The excitation energy of this state is $8\cdot44$ eV, whereas in the optical transition back to the ground state a photon with a vacuum ultraviolet (VUV) wavelength of 147 nm is emitted. Thus the detection and the determination of the polarisation of such photons requires the use of an VUV analyser. In Fig. 9 we show a scheme of our reflection-type VUV analyser, whose main components are a gold coated mirror with a surface flatness of $\lambda/20$ at 633 nm and a single channel electron multiplier which is coated with CsI to enhance its detection efficiency for VUV photons. A more detailed description of our two-mirror version, with which we can also measure the circular polarisation of VUV photons, is given elsewhere (Uhrig *et al.* 1994).
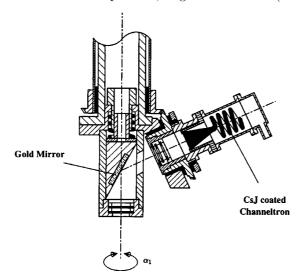

Fig. 9.   Diagram of the VUV analyser used for the 147 nm transition in Xe.

   For this collision system we could measure angle and energy scans of the spin up–down asymmetry $A_\perp$. The results are shown in Fig. 10 together with a distorted-wave Born approximation (DWBA) by Bartschat (1992), see also Bartschat and Madison (1987). Both theoretical curves have been calculated from the data of Bartschat (1992). The full curve shows the asymmetry $A_\perp$ calculated for an ideal analyser, whereas in the broken curve the actual analysing power of $0\cdot84$ has been taken into account. Since both curves do not differ much compared to the experimental uncertainties the analysing power can be considered of minor influence here. The general findings of Bartschat and Madison, which they derive from their DWBA calculation for Xe at $E = 20$ eV, show that at such energies it is mainly the singlet part of the wave functions (expressed in an intermediate coupling scheme) that is responsible for the excitation process.

Also, the amplitudes are only weakly influenced by the continuum spin–orbit interaction. As a result of these findings, only small spin effects and consequently small values of $A_\perp$ are expected. This is is confirmed by the small experimental values shown in Fig. 10 which are in good agreement with the theoretical curves.
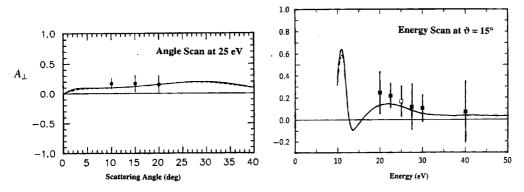
Fig. 10. Angle and energy scan of the spin up–down asymmetry parameter $A_\perp$ derived from electron–photon coincidences in Xe [excitation of the $5p^6 6s[\frac{3}{2}]_1(^3P_1)$ state] (Uhrig *et al.* 1994; Berkemeier 1994). Theoretical curves: DWBA calculations by Bartschat (1992) for an ideal analyser (full curves) and for the actual analysing power of $0 \cdot 84$ (dashed curves).

(3b) Stepwise Electron–Photon Excitation

Electron-impact excitation of metastable states cannot be investigated by the optical methods described before, because optical decay is suppressed. One can, however, use the stepwise electron–photon excitation method: the wavelength of a laser is tuned to a transition from the metastable state to another upper state which may then decay via an allowed transition (laser induced fluorescence). This method has been used in the past to study electron-impact excitation of Hg states (Lucas *et al.* 1982; MacGillivray and Standage 1988; Hanne *et al.* 1985). We used it recently to study electron-impact excitation of metastable Ne states (Fischer 1998).
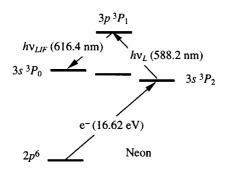
Fig. 11. Scheme for the stepwise electron–photon excitation in Ne.

The stepwise electron–photon excitation scheme is shown in Fig. 11. Ne atoms are excited by electron impact from the $2p^6$ ground state to the excited metastable $2p^5 3s\ ^3P_2$ state (excitation energy $16 \cdot 62$ eV). With laser photons

tuned to the 3s $^3P_2 \rightarrow$ 3p $^3P_1$ transition ($\lambda = 588 \cdot 2$ nm) laser induced fluorescence (LIF) of $616 \cdot 4$ nm photons is obtained. The final state (3s $^3P_0$) of this excitation scheme has $J = 0$ and thus the entire information about the alignment of the initial 3p $^3P_2$ state can be determined when polarised laser light is used and the polarisation of the laser induced fluorescence is measured.
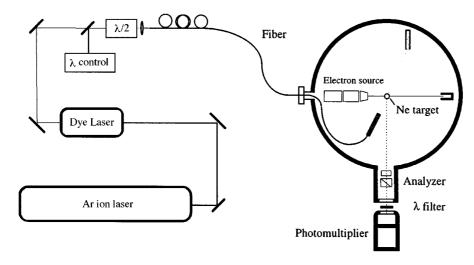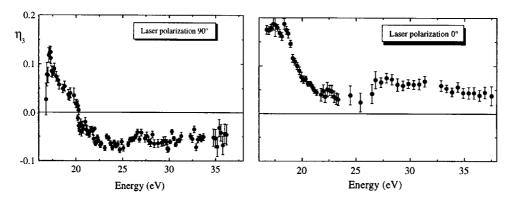

Fig. 12.   Experimental scheme for the stepwise electron–photon experiment with Ne.

The experimental scheme of that investigation is illustrated in Fig. 12. A tunable Rh 6G dye laser, pumped with an Ar$^+$ ion laser, provides the required linearly polarised photons with a wavelength of $588 \cdot 2$ nm. The laser light is fed into a fibre, where a rotatable $\lambda/2$ retarder allows one to rotate the linear polarisation. The wavelength is controlled by illuminating a Ne discharge tube. The discharge current depends strongly on the relative populations of the metastable Ne states and this is changed significantly if the laser is exactly tuned to the 3s $^3P_2 \rightarrow$ 3p $^3P_1$ transition ($\lambda = 588 \cdot 2$ nm). In the scattering chamber the photons are coupled out of the fibre and are directed onto a Ne gas target which is produced by a capillary array. Electrons from a conventional electron gun excite the Ne atoms and the LIF is detected perpendicular to the incident electron beam direction. The angle between the directions of the laser light and the analyser is 20°.

Results of the measurements of the linear polarisation of the LIF are shown in Fig. 13, where the laser polarisations are set perpendicular (90°) and parallel (0°) to the plane spanned by the electron and laser beam directions. Larger values of the polarisation (10–15%) at threshold ($16 \cdot 6$ eV) drop down to linear polarisations of no more than about $\pm 5\%$ for $E > 20$ eV.

From these data one can determine the ratios Q_2/Q_0 and Q_1/Q_0 of the integrated cross sections $Q_{|M|}$ for excitation of the different sublevels with magnetic quantum number M. However, this requires a careful analysis of the 'raw' data because the geometry of the excitation scheme has to be taken into account. If LS coupling holds the ratios Q_2/Q_0 and Q_1/Q_0 are not independent of each other because they depend only on the ratio $Q(1)/Q(0)$ for excitation

of the orbital magnetic sublevels $Q(M_L)$ of this P state. This analysis will be given in a forthcoming paper and is not shown here.

Fig. 13. Linear polarisation of laser induced fluorescence after stepwise electron–photon excitation in Ne (cf. Fig. 11 for the excitation scheme) for two settings of the laser polarisation (Fischer 1998).

The method of stepwise electron–photon excitation can also be used when excited states can radiate but polarisation analysis is complicated (e.g. for VUV photons), or if the high spectral resolution of photon analysers is necessary, e.g. to study rovibrationally resolved electron–molecule collisions.
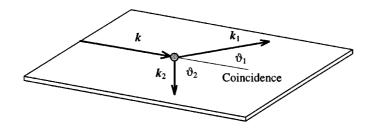

Fig. 14.   Scheme for an (e, 2e) experiment.

4. Spin-resolved Triple Differential Cross Sections of Xe

(4a) Introduction and Background

Recent experimental progress has made feasible (e, 2e) experiments involving polarised electrons, where the scattered and ejected electrons are detected in coincidence. A scheme for such an investigation is shown in Fig. 14. An incoming electron with wave vector k ionises an atom. The two outgoing electrons with wave vectors k_1 and k_2 are detected in coincidence for solid angles $\Delta\Omega_1$ and $\Delta\Omega_2$ and energy ΔE_1. Therefore, the (e, 2e) cross section is called a triple differential cross section (TDCS).

In a pioneering experiment, Baum *et al.* (1992) performed triple differential cross sections for polarised electrons incident on polarised lithium atoms. Because lithium is a very light target, the spin–orbit interaction is negligible and exchange following the Pauli principle is the dominant spin effect. Later, first results for

spin-resolved (e, 2e) experiments in Xe (Guo *et al.* 1996; Simon *et al.* 1995; Hanne 1996) and for inner-shell ionisation of (unpolarised) silver atoms were reported (Prinz *et al.* 1995). Whereas spin effects in K-shell ionisation of silver atoms are caused by the continuum spin–orbit interaction, the dominant mechanisms in the outer-shell ionisation of Xe is quite different as explained in the following.

Spin up–down asymmetries (cf. equation 2) in the excitation cross section of selected fine-structure levels of unpolarised targets excited by polarised electrons have become a well-known effect (Hanne 1983). It is observed if orbital orientation transfer and exchange between the two colliding electrons act simultaneously. Such asymmetries have also been observed in triple differential cross sections (TDCS) for ionisation of heavy rare gas atoms as anticipated earlier (Hanne 1992; Jones *et al.* 1994). In a coplanar (e, 2e) coincidence experiment, Xe atoms with a $5p^6\ {}^1S_0$ configuration of the valence electrons were ionised by collisions with polarised electrons with the $Xe^+(5p^5)$ ion being left in the ${}^2P_{1/2}$ or ${}^2P_{3/2}$ state. Significant spin up–down asymmetries in the TDCS are observed, if the fine-structure splitting is resolved. If relativistic effects can be ignored (except for the small fine-structure splitting), i.e. if pure LS coupling can be assumed, one would obtain (Hanne 1983)

$$S_A({}^2P_{1/2}) = -2S_A({}^2P_{3/2})\,. \qquad (4)$$

Consequently, no asymmetry can be observed if the fine-structure is not resolved, because the average over the two ionisation states would give $S_A = 0$, due to the fact that the cross section for the ${}^2P_{3/2}$ state is twice as large as that for the ${}^2P_{1/2}$ state in this approximation. It should be mentioned that this mechanism is significant also for ionisation of inner p shells, as has been shown recently both theoretically and experimentally (Jabubaßa-Amundsen 1995; Keller *et al.* 1996; Besch *et al.* 1998).

So far the investigations for spin-resolved (e, 2e) studies in Xe have concentrated on 147 eV electrons (Guo *et al.* 1996; Granitza *et al.* 1996; Dorn *et al.* 1997). Significant spin asymmetries are observed at this energy and first calculations (Jones *et al.* 1994; Madison *et al.* 1996; Granitza *et al.* 1996; Dorn *et al.* 1997) were in qualitative agreement with the observations. The quantitative agreement between experiment and theory was good in some cases, but severe discrepancies at other energies and angles have also been found. There was a variety of speculation about the reasons for these discrepancies. One explanation was that the interaction was not treated fully relativistically. Another idea was that the distorted-wave calculations used may work well for kinematics close to the Bethe ridge condition, where the momentum transferred to the residual ion is small, and may not work at geometries far off the Bethe ridge condition. Furthermore, the question was raised whether a proper treatment of exchange with the electrons of the residual ions—including capture where the incident electron is captured by the target and two target electrons are ejected—is important or not.

Here we review a recent investigation (Mette *et al.* 1998) that sheds more light on the reasons for the discrepancies between previous calculations and experiments. We have extended the experimental studies to energies between 40 eV and 200 eV to make a comparison with calculations for a broader range of energies possible. The results are compared with very recent calculations that

take exchange with the residual target electrons into account (Madison *et al.* 1998).

(4b) Experimental

Description of the experiment.   A scheme for our (e, 2e) experiment is shown in Fig. 15. A source of polarised electrons (photoemission from a GaAs crystal irradiated with circularly polarised light from a Pockels cell) provides an electron beam with a polarisation up to $P \approx 0 \cdot 4$ and currents of up to 250 nA at the target. Electron-impact ionisation of Xe atoms from a capillary beam source is studied by detecting scattered and ejected electrons in coincidence. With position sensitive detectors (PSD) at the exit of the electron spectrometers (CMA), we can detect different final energies simultaneously. A Mott detector operating at 120 keV is used to determine the initial polarisation. From an experimental point of view, (e, 2e) studies with a Xe target are of particular interest, since the fine-structure splitting of the ionic states of $1 \cdot 31$ eV can be resolved without major difficulties.
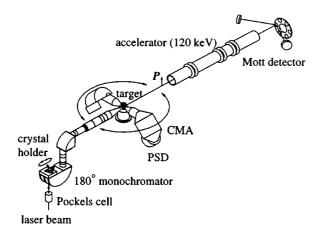

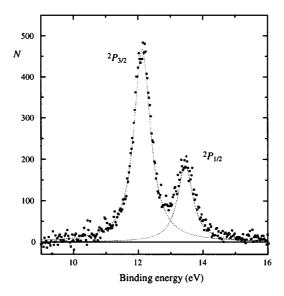**Fig. 15.**   Scheme for our (e, 2e) apparatus involving polarised electrons.

Energy binding spectra.   The energies E_1 and E_2 of two electrons which result from the same ionisation process are correlated by energy conservation and the energy resolution of the apparatus. Their sum is

$$E_1 + E_2 = E - E_{\mathrm{ion}} \pm \Delta E_{\mathrm{coinc}} , \tag{5}$$

where E is the incident energy, E_{ion} is the ionisation energy of the particular ionisation channel [$12 \cdot 12$ and $13 \cdot 433$ eV for $\mathrm{Xe}^+(\frac{3}{2})$ and $\mathrm{Xe}^+(\frac{1}{2})$ respectively] and $\Delta E_{\mathrm{coinc}}$ is the overall energy resolution of the coincidence experiment.

Our PSDs enable us to determine the energy of the two outgoing electrons. After some background corrections which are described elsewhere (Mette *et al.* 1998), we obtain the number of true coincidences for which E_1+E_2 is constant with an energy integration of $\Delta E = 5$ eV for E_1. Because we use polarised electrons, this number may depend on their polarisation P. If we plot the resulting

numbers $N(\pm P)$ of true coincidences versus the binding energy $E - (E_1 + E_2)$, we get the result shown in Fig. 16. The two different channels are clearly separated in the binding energy spectrum and the asymmetry (2) can be evaluated for each ionisation channel by setting proper integration windows to avoid overlap with the wrong channel.

Fig. 16. Energy binding spectrum of Xe at $E = 100$ eV, ϑ_1 $= \vartheta_2 = 40°$ and 'symmetric energy sharing' integrated over $41 < E_1,\ E_2 < 46$ eV. A fit indicates the true separation of the two peaks.

(4c) Results and Discussion

Results that have been obtained with the apparatus shown in Fig. 15 together with the theoretical results are presented in Figs 17 and 18. Exchange enters a theoretical calculation in two different ways. The first exchange effect is the exchange amplitude which represents the effects of exchange between projectile electron and ionised electron. All of the original theoretical calculations (Jones *et al.* 1994; Granitza *et al.* 1996; Madison *et al.* 1996) contained an evaluation of the exchange amplitude. The second exchange effect results from the projectile electron interchanging with the residual target electrons. Classically, this effect alters the path of the projectile and, as a result, has been labeled 'exchange distortion'. The effect of exchange distortion was examined by Madison *et al.* (1998) and it was found to be important for some kinematical conditions and not others. It was also found that exchange distortion was important for the two final state electrons, but not important for the incident projectile. Here, results are presented both with and without exchange distortion.

Results for $E = 40$, 60 and 100 eV with $\vartheta_1 = 40°$ and symmetric energy sharing are shown in Fig. 17. The case of symmetric energy sharing ($E_1 = E_2$) is particularly interesting, since the asymmetry must vanish due to symmetry when the angles ϑ_1 and ϑ_2 are equal, i.e. in our case at $\vartheta_2 = 40°$. In the original
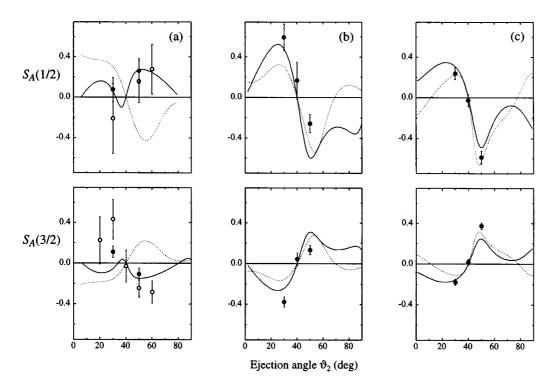
Fig. 17. Spin up–down asymmetry function $S_A(J)$ in the TDCS for electron-impact ionisation of the ^{2}P ($J = \frac{1}{2}, \frac{3}{2}$) states of Xe$^+$ with symmetric energy sharing ($E_1 = E_2$) and $\vartheta_1 = 40°$ at (a) $E = 40$ eV, (b) $E = 60$ eV and (c) $E = 100$ eV around the zero crossing at $\vartheta_2 = 40°$. Experimental results: solid circles, Mette *et al.* (1998); open circles, Simon *et al.* (1995). Calculations: solid curves, DWBA with exchange distortion; dotted curves, DWBA without exchange distortion (Madison *et al.* 1998).

theoretical approaches (Jones 1995; Mazevet 1995; Madison 1996) the asymmetry had the wrong sign near the required zero crossing, whereas at energies above 60 eV the sign was predicted correctly. Fig. 17 reveals that the severe discrepancy between theory and experiment at 40 eV is considerably reduced if exchange between the scattered electrons and the electrons of the Xe$^+$ ion is included in the calculation. This indicates that a proper treatment of such effects is very important to get a satisfactory description of the problem.

Discrepancies between previous theoretical calculations and experimental data have also been obtained by the Canberra group at certain kinematic situations for $E = 147$ eV. One possible explanation for the problem was that the calculations were not performed relativistically. However, neither the use of relativistic target orbitals (Madison *et al.* 1996; Granitza *et al.* 1996), nor the inclusion of continuum spin–orbit interactions (Dorn *et al.* 1997), provided a significant improvement in the agreement between experiment and theory.

Another explanation was that the distorted-wave approach fails to give satisfactory results for kinematic situations where a significant momentum $\Delta \boldsymbol{p} = \hbar\Delta \boldsymbol{k}$ is transferred to the ion. The scattering angle ϑ_1 and the energy E_1 can be chosen such that there exists an ejection angle ϑ_2 for which the wave vectors

$\boldsymbol{k}$, $\boldsymbol{k}_1$ and $\boldsymbol{k}_2$ of incident, scattered and ejected electron, respectively, obey the relation

$$\boldsymbol{k} = \boldsymbol{k}_1 + \boldsymbol{k}_2 \,, \qquad\qquad (6)$$

i.e. for which the initial momentum of the incoming electron is equal to the sum of the momenta of two outgoing electrons. If the target electron was initially at rest, the condition shown in equation (6) would obey momentum conservation by the colliding electrons with no transfer of angular momentum to the target. At given energies $E_1 = \hbar^2 k_1{}^2/2m$ and $E_2 = \hbar^2 k_2{}^2/2m$, one can calculate from equation (5) an angle ϑ_1 for which the relation

$$k_2^2 = |\boldsymbol{k} - \boldsymbol{k}_1|^2 = k^2 + k_1^2 - 2kk_1\cos\vartheta_1 \qquad\qquad (7)$$

holds. This is called the Bethe ridge region (McCarthy and Weigold 1995).

In Fig. 18 results are shown for $E = 100$ and 200 eV with asymmetric energies $E_1 > E_2$. For $E = 100$ eV and $E_1 \approx 60$ eV (which gives $E_2 \approx 28$ eV), we obtain from equation (6) a scattering angle $\vartheta_1 = 31 \cdot 6°$, whereas for $E =$
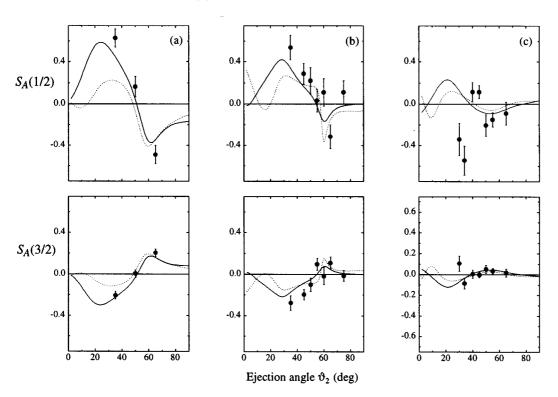

Fig. 18. Spin up–down asymmetry function $S_A(J)$ in the TDCS for electron-impact ionisation of the $5p^5$ ^{2}P ($J = \frac{1}{2}$, $\frac{3}{2}$) states of Xe$^+$ with asymmetric energy sharing ($E_1 > E_2$) at (a) $E = 100$ eV, $E_1 = 60$ eV, $\vartheta_1 = 32°$, (b) $E = 200$ eV, $E_1 = 138$ eV, $\vartheta_1 = 30°$ and (c) $E = 200$ eV, $E_1 = 138$ eV, $\vartheta_1 = 20°$. Experimental data: solid circles, Mette *et al.* (1998). Calculations: solid curves, DWBA with exchange distortion; dotted curves, DWBA without exchange distortion (Madison *et al.* 1998).

200 eV, $E_1 \approx 138$ eV ($E_2 \approx 50$ eV) we get $\vartheta_1 \approx 30°$. Thus the kinematic situations in Figs 18a and 18b are very close to the Bethe ridge regime, and the agreement between experiment and theory is very good. For $\vartheta_1 = 20°$ (Fig. 18c), the agreement is less satisfactory for the smaller ejection angles ($\vartheta_2 < 50°$). However, a single observation does not provide confirmation of the statement that the theory is poor for kinematic situations far off the Bethe ridge condition. Additional measurements would have to be performed to further clarify this point.

5. Conclusions

The use of polarised electrons and photons allows one to probe collisions of electrons with atoms in great detail, in particular by measurement of various spin asymmetries in electron–photon and (e, 2e) coincidences. In particular, these methods can help

- to study separately reaction channels over which the average is usually performed and, in processes not too complicated, to obtain the maximum possible information,
- to study the influence of the weak spin–orbit interaction, and to disentangle it from exchange and the Coulomb interaction by which it is usually masked.

Electron–photon coincidences provide a very sensitive test of inelastic electron–atom collision calculations. For heavy atoms such as Hg these are not yet available, but it is expected that substantial computational progress will provide data that are as accurate as those for light targets such as Na.

The population of magnetic sublevels of metastable states can be successfully determined by means of stepwise electron–photon excitation, a method that can be also used for VUV transitions where light polarisation analysis is complicated or for collisions where a high spectral resolution must be achieved.

The use of polarised electrons in (e, 2e) collisions provides a powerful tool for unraveling competing spin- and non spin-dependent effects in the ionisation process. The fine-structure effect is the natural contribution of exchange to the asymmetry parameter S_A even for complex targets such as Xe atoms. For such a heavy target, relativistic effects certainly play a role, but they cannot account for the fact that the agreement between experiment and previous theories for some kinematics is not satisfactory. Recent calculations of Madison *et al.* (1998) that include exchange distortion with the target electrons of the residual Xe^+ ion are in much better agreement. It is thus shown that a proper treatment of exchange is more important for obtaining satisfactory predictions than the inclusion of relativistic effects.

References

Andersen, N., Bartschat, K., Uhrig, M., and Hanne, G. F. (1996). *Phys. Rev. Lett.* **76**, 208.
Andersen, N., Bartschat, K., Broad, J. T., and Hertel, I. V. (1997). *Phys. Rep.* **279**, 251.
Bartschat, K. (1988). Personal communication.

Bartschat, K. (1989). *Phys. Rep.* **180**, 1.

Bartschat, K. (1992). Personal communication, data based on Bartschat and Madison (1987).

Bartschat, K., and Madison, D. H. (1987). *J. Phys.* B **20**, 5839 [erratum (1992). *J. Phys.* B **25**, 1361].

Bartschat, K., Madison, D. H., and Hanne, G. F. (1985). *J. Phys.* B **18**, 1847.

Baum, G., Blask, W., Freienstein, P., Frost, L., Hesse, S., Raith, W., Rappolt, P., and Streun, M. (1992). *Phys. Rev. Lett.* **69**, 3037.

Berkemeier, M. (1994). Diploma Thesis, Universität Münster.

Besch, K.-H., Sauter, M., and Nakel, W. (1998). *Phys. Rev.* A **58**, R2638.

Dorn, A., Elliott, A., Guo, X., Hurn, J., Lower, J., Mazevet, S., McCarthy, I. E., Shen, Y., and Weigold, E. (1997). *J. Phys.* B **30**, 4097.

Fischer, S. (1998). PhD Thesis, Universität Münster.

Goeke, J., Hanne, G. F., and Kessler, J. (1989). *J. Phys.* B **22**, 1075.

Granitza, B., Guo, X., Hurn, J. M., Lower, J., Mazevet, S., McCarthy, I. E., Shen, Y., and Weigold, E. (1996). *Aust. J. Phys.* **49**, 383.

Guo, X., Hurn, J. M., Lower, J., Mazevet, S., Shen, Y., Weigold, E., Granitza, B., and McCarthy, I. E. (1996). *Phys. Rev. Lett.* **76**, 1228.

Hanne, G. F. (1983). *Phys. Rep.* **95**, 95.

Hanne, G. F. (1992). *In* 'Correlations and Polarisation in Electronic and Atomic Collisions and (e, 2e) Reactions', IOP Conf. Series Number 122 (Eds P. J. O. Teubner and E. Weigold), p. 15 (IOP: Bristol).

Hanne, G. F. (1996). *Can. J. Phys.* **74**, 811.

Hanne, G. F., Nickich, V., and Sohn, M. (1985). *J. Phys.* B **18**, 2037.

Jakubaßa-Amundsen, D. H. (1995). *J. Phys.* B **28**, 259.

Jones, S. (1995). Personal communication, data based on Jones *et al.* (1994).

Jones, S., Madison, D. H., and Hanne, G. F. (1994). *Phys. Rev. Lett.* **72**, 2554.

Keller, S., Dreizler, R. M., Ast, H., Whelan, C. T., and Walters, H. R. J. (1996). *Phys. Rev.* A **53**, 2295.

Lucas, C. W., MacGillivray, W. R., and Standage, M. C. (1982). *J. Phys.* B **15**, 1883.

McCarthy, I. E., and Weigold, E. (1995). 'Electron–Atom Collisions', p. 263 (Cambridge University Press).

MacGillivray, W. R., and Standage, M. C. (1988). *Phys. Rep.* **168**, 1.

Madison, D. H. (1996). Personal communication, data based on Madison *et al.* (1996).

Madison, D. H., Kravtsov, V. D., Jones, S., and McEachran, R. P. (1996). *Phys. Rev.* A **53**, 1996.

Madison, D. H., Kravtsov, V. D., and Mazevet, S. (1998). *J. Phys.* B **31**, L17.

Mazevet, S. (1995). Personal communication, data based on Granitza *et al.* (1996).

Mette, C., Simon, T., Herting, C., Hanne, G. F., and Madison, D. H. (1998). *J. Phys.* B **31**, 4689.

Prinz, H.-Th., Besch, K.-H., and Nakel, W. (1995). *Phys. Rev. Lett.* **74**, 243.

Simon, T., Mette, C., and Hanne, G. F. (1995). ICPEAC XIX, Abstracts of Contributed Papers (Eds J. B. A. Mitchell *et al.*), p. 224 (Whistler, British Columbia).

Sohn, M., and Hanne, G. F. (1992). *J. Phys.* B **25**, 4627.

Uhrig, M., Hanne, G. F., and Kessler, J. (1994). *J. Phys.* B **27**, 4009.